

# High purity bright single photon source

J. S. Neergaard-Nielsen, B. Melholt Nielsen, H. Takahashi\*,  
A. I. Vistnes<sup>†</sup> and E. S. Polzik

*QUANTOP, Danish National Research Foundation Center for Quantum Optics,  
Niels Bohr Institute, University of Copenhagen, DK 2100, Denmark*

\* *Permanent address: Department of Applied Physics, The University of Tokyo 7-3-1 Hongo,  
Bunkyo-ku, Tokyo 113-8656, Japan, and National Institute of Information and  
Communications Technology, 4-2-1 Nukui-Kita, Koganei, Tokyo 184-8795, Japan*

<sup>†</sup> *Permanent address: Department of Physics, University of Oslo, Postboks 1048, Blindern,  
0316 Oslo, Norway*

[jneergrd@nbi.dk](mailto:jneergrd@nbi.dk)

**Abstract:** Using cavity-enhanced non-degenerate parametric down-conversion, we have built a frequency tunable source of heralded single photons with a narrow bandwidth of 8 MHz, making it compatible with atomic quantum memories. The photon state is 70% pure single photon as characterized by a tomographic measurement and reconstruction of the quantum state, revealing a clearly negative Wigner function. Furthermore, it has a spectral brightness of  $\sim 1,500$  photons/s per MHz bandwidth, making it one of the brightest single photon sources available. We also investigate the correlation function of the down-converted fields using a combination of two very distinct detection methods; photon counting and homodyne measurement.

© 2021 Optical Society of America

**OCIS codes:** (120.2920) Homodyning; (230.6080) Sources; (270.5290) Photon statistics.

---

## References and links

1. N. Gisin, G. Ribordy, W. Tittel, and H. Zbinden, "Quantum cryptography," *Rev. Mod. Phys.* **74**, 145–195 (2002).
2. E. Knill, R. Laflamme, and G. J. Milburn, "A scheme for efficient quantum computation with linear optics," *Nature* **409**, 46–52 (2001).
3. B. Julsgaard, J. Sherson, J. I. Cirac, J. Fiurášek, and E. S. Polzik, "Experimental demonstration of quantum memory for light," *Nature* **432**, 482–486 (2004).
4. J. F. Sherson, H. Krauter, R. K. Olsson, B. Julsgaard, K. Hammerer, I. Cirac, and E. S. Polzik, "Quantum teleportation between light and matter," *Nature* **443**, 557–560 (2006).
5. P. Michler, A. Kiraz, C. Becher, W. V. Schoenfeld, P. M. Petroff, L. Zhang, E. Hu, and A. Imamoglu, "A quantum dot single-photon turnstile device," *Science* **290**, 2282–2285 (2000).
6. Z. Yuan, B. E. Kardynal, R. M. Stevenson, A. J. Shields, C. J. Lobo, K. Cooper, N. S. Beattie, D. A. Ritchie, and M. Pepper, "Electrically driven single-photon source," *Science* **295**, 102–105 (2002).
7. C. Kurtsiefer, S. Mayer, P. Zarda, and H. Weinfurter, "Stable solid-state source of single photons," *Phys. Rev. Lett.* **85**, 290–293 (2000).
8. R. Brouri, A. Beveratos, J.-P. Poizat, and P. Grangier, "Photon antibunching in the fluorescence of individual color centers in diamond," *Opt. Lett.* **25**, 1294–1296 (2000).
9. B. Lounis and W. E. Moerner, "Single photons on demand from a single molecule at room temperature," *Nature* **407**, 491–493 (2000).
10. B. Darquie, M. P. A. Jones, J. Dingjan, J. Beugnon, S. Bergamini, Y. Sortais, G. Messin, A. Browaeys, and P. Grangier, "Controlled single-photon emission from a single trapped two-level atom," *Science* **309**, 454–456 (2005).
11. M. Pelton, C. Santori, J. Vuc̆ković, B. Zhang, G. S. Solomon, J. Plant, and Y. Yamamoto, "Efficient source of single photons: A single quantum dot in a micropost microcavity," *Phys. Rev. Lett.* **89**, 233602 (2002).
12. J. McKeever, A. Boca, A. D. Boozer, R. Miller, J. R. Buck, A. Kuzmich, and H. J. Kimble, "Deterministic generation of single photons from one atom trapped in a cavity," *Science* **303**, 1992–1994 (2004).

13. M. Keller, B. Lange, K. Hayasaka, W. Lange, and H. Walther, "Continuous generation of single photons with controlled waveform in an ion-trap cavity system," *Nature* **431**, 1075–1078 (2004).
14. T. Wilk, S. C. Webster, H. P. Specht, G. Rempe, and A. Kuhn, "Polarization-controlled single photons," *Phys. Rev. Lett.* **98**, 063601 (2007).
15. D. N. Matsukevich, T. Chaneliere, S. D. Jenkins, S.-Y. Lan, T. A. B. Kennedy, and A. Kuzmich, "Deterministic single photons via conditional quantum evolution," *Phys. Rev. Lett.* **97**, 013601 (2006).
16. J. K. Thompson, J. Simon, H. Loh, and V. Vuletic, "A high-brightness source of narrowband, identical-photon pairs," *Science* **313**, 74–77 (2006).
17. S. Chen, Y.-A. Chen, T. Strassel, Z.-S. Yuan, B. Zhao, J. Schmiedmayer, and J.-W. Pan, "Deterministic and storable single-photon source based on a quantum memory," *Phys. Rev. Lett.* **97**, 173004 (2006).
18. C. K. Hong and L. Mandel, "Experimental realization of a localized one-photon state," *Phys. Rev. Lett.* **56**, 58–60 (1986).
19. P. G. Kwiat, K. Mattle, H. Weinfurter, A. Zeilinger, A. V. Sergienko, and Y. Shih, "New high-intensity source of polarization-entangled photon pairs," *Phys. Rev. Lett.* **75**, 4337–4341 (1995).
20. A. I. Lvovsky, H. Hansen, T. Aichele, O. Benson, J. Mlynek, and S. Schiller, "Quantum state reconstruction of the single-photon fock state," *Phys. Rev. Lett.* **87**, 050402 (2001).
21. T. Pittman, B. Jacobs, and J. Franson, "Heralding single photons from pulsed parametric down-conversion," *Opt. Commun.* **246**, 545–550 (2005).
22. A. B. U'Ren, C. Silberhorn, K. Banaszek, and I. A. Walmsley, "Efficient conditional preparation of high-fidelity single photon states for fiber-optic quantum networks," *Phys. Rev. Lett.* **93**, 093601 (2004).
23. J. Fulconis, O. Alibart, W. Wadsworth, P. Russell, and J. Rarity, "High brightness single mode source of correlated photon pairs using a photonic crystal fiber," *Opt. Express* **13**, 7572–7582 (2005).
24. Y. J. Lu and Z. Y. Ou, "Optical parametric oscillator far below threshold: Experiment versus theory," *Phys. Rev. A* **62**, 033804 (2000).
25. H. Wang, T. Horikiri, and T. Kobayashi, "Polarization-entangled mode-locked photons from cavity-enhanced spontaneous parametric down-conversion," *Phys. Rev. A* **70**, 043804 (2004).
26. C. E. Kuklewicz, F. N. C. Wong, and J. H. Shapiro, "Time-bin-modulated biphotons from cavity-enhanced down-conversion," *Phys. Rev. Lett.* **97**, 223601 (2006).
27. A. Zavatta, S. Viciani, and M. Bellini, "Tomographic reconstruction of the single-photon fock state by high-frequency homodyne detection," *Phys. Rev. A* **70**, 053821 (2004).
28. A. Ourjoumtsev, R. Tualle-Broui, and P. Grangier, "Quantum homodyne tomography of a two-photon fock state," *Phys. Rev. Lett.* **96**, 213601 (2006).
29. P. D. Drummond and M. D. Reid, "Correlations in nondegenerate parametric oscillation. II. Below threshold results," *Phys. Rev. A* **41**, 3930–3949 (1990).
30. C. Schori, J. L. Sørensen, and E. S. Polzik, "Narrow-band frequency tunable light source of continuous quadrature entanglement," *Phys. Rev. A* **66**, 033802 (2002).
31. J. S. Neergaard-Nielsen, B. M. Nielsen, C. Hettich, K. Mølmer, and E. S. Polzik, "Generation of a superposition of odd photon number states for quantum information networks," *Phys. Rev. Lett.* **97**, 083604 (2006).
32. A. E. B. Nielsen and K. Mølmer, "Single-photon-state generation from a continuous-wave nondegenerate optical parametric oscillator," *Phys. Rev. A* **75**, 023806 (2007).
33. Z. Y. Ou and H. J. Kimble, "Probability distribution of photoelectric currents in photodetection processes and its connection to the measurement of a quantum state," *Phys. Rev. A* **52**, 3126 (1995).
34. A. I. Lvovsky, "Iterative maximum-likelihood reconstruction in quantum homodyne tomography," *J. Opt. B: Quantum and Semiclassical Optics* **6**, S556–S559 (2004).
35. N. B. Grosse, T. Symul, M. Stobińska, T. C. Ralph, and P. K. Lam, "Measuring photon anti-bunching from continuous variable sideband squeezing," [quant-ph/0609033](https://arxiv.org/abs/quant-ph/0609033).
36. G. T. Foster, W. P. Smith, J. E. Reiner, and L. A. Orozco, "Time-dependent electric field fluctuations at the subphoton level," *Phys. Rev. A* **66**, 033807 (2002).

## 1. Introduction

Pure single photon states produced efficiently and at a high rate are highly desirable for practical implementations of various quantum information processing protocols, in particular in quantum cryptography [1], quantum computing with linear optics [2], and for testing quantum memories [3, 4]. The latter applications require at the same time compatibility with some kind of a quantum memory. Different approaches towards generation of a single photon state have been implemented in a number of physical systems. It should be noted that in many instances a source is claimed to be "a single photon source" based just on the property of antibunching, i.e., on the low rate of two-photon contribution compared to a single photon part. Such

property should be combined with the likewise low contribution of the vacuum state, in order to claim a high-purity truly single photon source which is the aim of the present work. Single emitters usually suffer from low purity due to small collection efficiency for light. For example, quantum dot based sources [5, 6], color centres in diamond [7, 8], single molecules [9], or a single atom [10] have the detection efficiency/purity at best at a few percent level. Placing single emitters inside high-Q cavities improves the purity dramatically. However, even complex state-of-the-art experiments still have limited overall collection efficiency and thus low purity. The best results with quantum dots [11] show 8% collection efficiency/purity. Besides, quantum dots usually emit light in a several GHz bandwidth. The best efforts with cavity-QED with atoms or ions yield 30-40% efficiency just outside the cavity and the overall efficiency/purity at 10-20% level [12, 13, 14]. Recently atomic ensembles have been used to produce non-classical light [15, 16, 17], however, the light collection efficiency does not exceed a few percent even when atoms are placed inside a cavity [16]. Parametric down-conversion in free space nonlinear crystals or waveguides [18, 19, 20, 21, 22, 23] has been widely used for generation of heralded photon pulses. The major disadvantage of parametric down-conversion is the random arrival time of the photons – the source is not deterministic. However, this is compensated by many attractive properties like well-defined wavelength, high collection efficiency, and non-cryogenic experimental setups. The standard pulsed, single-pass down-conversion process suffers from a limited photon generation rate which must be kept low to avoid pulses containing two photons, which is detrimental for quantum information applications. The bandwidth of the down-conversion is typically several nanometers, which means that the spectral brightness (the number of photons per MHz per second) is below one. This poses a serious limitation to the feasibility of interaction with atomic systems, where linewidths are on the MHz scale. To overcome this problem, the nonlinear crystal can be placed inside an optical cavity which serves to enhance the down-conversion process and limit the bandwidth of the output to that of the cavity [24]. Furthermore, the spatial field mode is defined by the cavity as well, so no additional spatial filtering is needed. Various studies on this type of setup have been performed, and the results do indeed show a marked increase in the attained spectral brightness [24, 25, 26].

In this paper we present our scheme for generation of heralded single photons with a very high purity and spectral brightness, and we perform homodyne tomography on these photons, which gives a complete image of the state of the source. Tomographic measurements of single photons have previously been performed in the pulsed regime [20, 27, 28] but not for continuously pumped systems. In overview, we operate an optical parametric oscillator (OPO) with a pump level which is far below the oscillation threshold; in effect this is just cavity-enhancement of the spontaneous parametric down-conversion of the nonlinear crystal. The ordinary phase matching bandwidth of the down-conversion process is several nm, but the cavity effectively inhibits down-conversion into frequencies which do not fulfill the resonance condition. Thus, the output of the OPO consists of several narrow-band frequency modes separated by the free spectral range (FSR) of the cavity. By appropriately filtering the output, we can obtain with high efficiency a single photon in a specific one of those modes conditioned on the detection of a trigger photon. The bandwidth of this photon will then be the cavity bandwidth which is very narrow compared to the phase matching bandwidth.

## 2. Experiment

The OPO, as well as the rest of the setup, is depicted in Fig. 1. It is a bow-tie type cavity with a length of 81 cm corresponding to a FSR of 370 MHz. Centered between two 5 cm curvature mirrors is a 10 mm long PPKTP crystal which is periodically poled for noncritical phase matching around 860 nm. The output coupler has a transmission of  $T = 12.5\%$ , and the total internal losses are  $L = 0.4\%$ , giving a cavity HWHM bandwidth of  $\gamma_{1/2} = 2\pi \cdot 4.0$  MHz and an

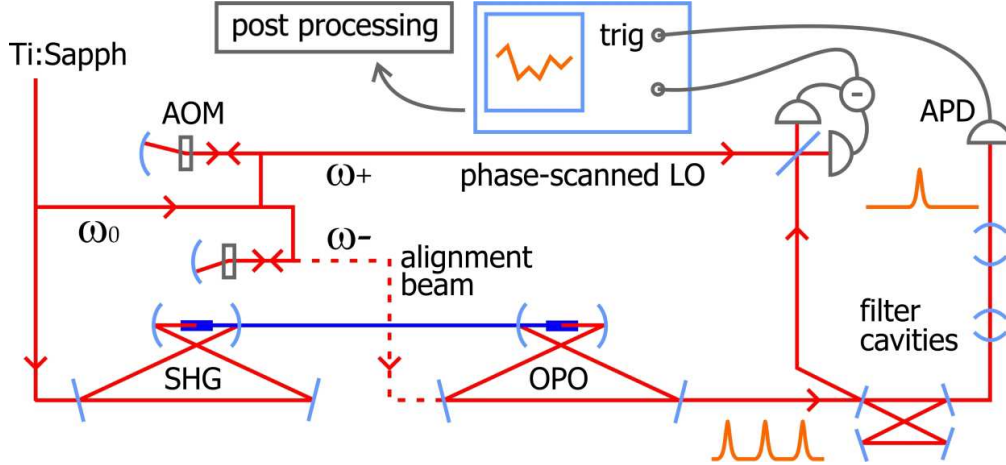


Fig. 1. (Color online) Setup diagram. The second harmonic generator (SHG) pumps the optical parametric oscillator (OPO). The filter cavities should allow only a single mode (at frequency  $\omega_-$ ) to reach the single photon counting avalanche photo diode (APD). Two acousto optic modulators (AOM) shift the main frequency to  $\omega_-$  and  $\omega_+$  - the latter is used for the local oscillator (LO) of the homodyne measurement, the former for an alignment beam, which is used to bring all cavities resonant with  $\omega_-$  but which is blocked during measurement.

escape efficiency  $\eta_{\text{esc}} = T/(T + L) = 0.97$ . With an effective nonlinearity  $E_{\text{NL}} \approx 0.020 \text{ W}^{-1}$ , the threshold pump power for oscillation is around  $P_{\text{thr}} = (T + L)^2/4E_{\text{NL}} = 210 \text{ mW}$ . The blue pump (430 nm) is generated by frequency doubling the main Ti:Sapph laser in a second harmonic generator (SHG) of similar geometry as the OPO, but with a  $\text{KNbO}_3$  crystal as the nonlinear medium. For single photon generation the pump should be rather weak to inhibit the population of higher photon numbers. The pumping strength is quantized as the pump parameter  $\varepsilon = \sqrt{P_b/P_{\text{thr}}}$ , where  $P_b$  is the blue pump power. This pump parameter is most easily inferred by observing the parametric gain,  $G = 1/(1 - \varepsilon)^2$  of a beam of half the pump frequency seeded into the OPO.

The frequency spectrum of the OPO is illustrated in Fig. 2. With no seed beam, the output field in the degenerate frequency mode (half pump frequency) is quadrature-squeezed vacuum, whereas the non-degenerate modes taken individually are thermal states. They are, however, pairwise correlated symmetrically around the degenerate frequency. In the weak pump regime this means that for each down-converted photon in the  $\omega_-$  mode one FSR below the degenerate frequency, there is a twin photon in the  $\omega_+$  mode one FSR above. In the time domain, the field operator correlations for the two modes are given by [29]:

$$\begin{aligned}
 \langle \hat{a}_{\pm}(t)\hat{a}_{\mp}(t') \rangle &= \frac{\lambda^2 - \mu^2}{4} \left( \frac{e^{-\mu|t-t'|}}{2\mu} + \frac{e^{-\lambda|t-t'|}}{2\lambda} \right) \\
 \langle \hat{a}_{\pm}^{\dagger}(t)\hat{a}_{\pm}(t') \rangle &= \frac{\lambda^2 - \mu^2}{4} \left( \frac{e^{-\mu|t-t'|}}{2\mu} - \frac{e^{-\lambda|t-t'|}}{2\lambda} \right) \\
 \langle \hat{a}_{\pm}(t)\hat{a}_{\pm}(t') \rangle &= \langle \hat{a}_{\pm}^{\dagger}(t)\hat{a}_{\mp}(t') \rangle = 0,
 \end{aligned} \tag{1}$$

with

$$\lambda = \gamma_{1/2}(1 + \varepsilon), \quad \mu = \gamma_{1/2}(1 - \varepsilon).$$

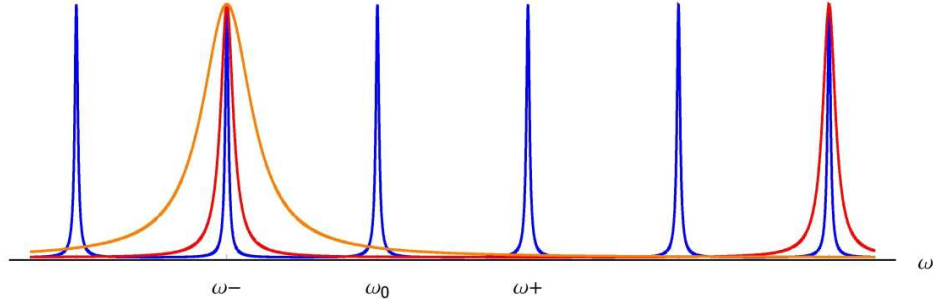


Fig. 2. (Color online) Schematic illustration of the frequency mode spectrum of the OPO (blue). The pump at frequency  $2\omega_0$  induces down-conversion into these and several other neighbouring modes. The  $\omega_-$  and  $\omega_+$  modes are correlated, and they are separated on the first filter cavity which is resonant on  $\omega_-$  and reflects  $\omega_+$  (red). Subsequent filters, of which one is depicted (orange), serves to further suppress uncorrelated modes in the trigger arm.

Thus, if we can spatially separate the two frequency modes and detect the  $\omega_-$  photon on a single photon detector we have heralded the existence of an  $\omega_+$  photon within a temporal mode determined by these correlations. This separation is done using an empty cavity which works as a frequency filter; the FSR is four times that of the OPO, so with the cavity resonant on  $\omega_-$ , the  $\omega_+$  mode will be almost completely reflected. With this scheme the non-degenerate OPO has previously been used to produce highly quadrature entangled EPR beams [30]. Because of the wide phase matching bandwidth, many other modes than  $\omega_-$  will slip through the first filter cavity. Hence we need two more filter cavities with different FSR and a 0.3 nm interference filter on the way towards the photon counting avalanche photo diode (APD). If any photons uncorrelated with the  $\omega_+$  photons arrive at the APD, the  $\omega_+$  state conditioned on these “false” detections will be the original thermal state instead of a single photon. The spectral arrangement of these filters is illustrated in Fig. 2. The lengths of the cavities are 210 mm, 3.7 mm, and 12 mm, and the FWHM bandwidths are roughly 48 MHz, 270 MHz, and 96 MHz, respectively. To keep all cavities (OPO + filters) on resonance with the  $\omega_-$  frequency, we monitor the total transmission (the APD click rate) and keep it on maximum using individual error signals from each cavity obtained by dithering them at different frequencies. We recently employed the same series of filter cavities and APD to herald the generation of a photon subtracted squeezed vacuum state (a “Schrödinger kitten“) [31].

With the  $\omega_-$  and  $\omega_+$  modes thus separated and with the APD click heralding an  $\omega_+$  photon, the existence of this photon must be confirmed. Instead of just measuring the arrival of the photons on another APD, we do a homodyne measurement of the field by mixing it on a 50/50 beam splitter with a strong local oscillator (LO) and subsequently recording the difference of the photocurrents measured in the two arms. The LO has been shifted by 370 MHz to the center frequency of the  $\omega_+$  mode by sending part of the main laser beam through an AOM (acousto optic modulator). The detector employs two Hamamatsu photo diodes (special production of the S5971 type) with a specified quantum efficiency of 98%. It has a bandwidth of more than 100 MHz, and with 1.5 mW light on each diode the shot noise is 10 dB above the electronic noise floor. The output of the detector goes to a fast digital oscilloscope which samples the signal at 500 MS/s for a period of 2  $\mu$ s around each APD trigger event. By repeating the state generation and measurement several thousand times, statistics about the quadrature distribution of the output state is build up. We scan the phase of the local oscillator to observe all quadrature phases, but as expected the distribution is completely phase invariant.



In the post-processing of the recorded noise, we have to extract the conditional quadrature information from the thermal state background. This is done by applying a temporal mode function filter,  $f_s(t)$ , to the noise traces and afterwards integrate the traces over time. This leaves us with a single mode quadrature value corresponding to the operator

$$\hat{a}_s = \int f_s(t') \left[ \sqrt{\eta_s} \hat{a}_+(t') + \sqrt{1 - \eta_s} \hat{a}_{+,vac}(t') \right] dt' , \quad (2)$$

where  $\eta_s$  is the total generation and detection efficiency of the signal, and the vacuum mode is added to maintain the commutator relations. For the very low gain regime ( $\epsilon \ll 1$ ), the optimal field mode function for high single photon fidelity is simply the double-sided exponential [24, 32]

$$f_{s,opt}(t) = \sqrt{\gamma_1/2} e^{-\gamma_1/2|t-t_c|} , \quad (3)$$

with  $t_c$  the time of the trigger event. For high gains the problem of finding the optimal mode function becomes somewhat more involved – see [32] – but this is not a big concern at the low gains at which we operate. Due to the filtering of the trigger photon, the correlations between trigger and signal will be smeared out, so our optimal mode function should be a bit wider and rounded off. However, since the narrowest trigger filter cavity has a bandwidth 6 times wider than that of the OPO, the effect is not very significant, and using just the first approximation to the optimal mode function above, we obtain fidelities quite similar to those obtained using more precise mode functions. The procedure of post-processing the homodyne photo current with temporal filtering is equivalent to performing the homodyne measurement with a pulsed LO of the same shape as the mode function. However, the shaping of the LO will have to be initiated by the trigger photon detection, and until the shaped LO is ready, the signal photon must be delayed so that the two fields reach the beam splitter simultaneously. See [33] for a detailed account of the problem of temporal/spectral mode matching in continuous-wave homodyning.

### 3. Analysis

For the data presented in this paper, we performed a total number of 180,000 generations/measurements of the single photon state. The measured parametric gain was about  $G \approx 1.2$ , corresponding to a pump parameter  $\epsilon \approx 0.09 \ll 1$  (the effective blue pump power is  $\approx 1.7$  mW). Applying the mode function (3) to the noise traces, we get the quadrature distribution shown in Fig. 3(a,b). A simple fit to the single photon quadrature distribution admixed with vacuum,  $\eta|\langle q|1\rangle|^2 + (1 - \eta)|\langle q|0\rangle|^2$ , shows that our data is consistent with a single photon state which has been detected with an efficiency of  $\eta = 62\%$ . Based on the measured quadrature values and corresponding phases, we have reconstructed the density matrix and Wigner function of the generated state, using the maximum likelihood tomographic reconstruction method [34]. The results are presented in Fig. 3(c,d). We see that our state consists almost entirely of  $n = 0$  and  $n = 1$  number states, with an  $n = 1$  population of 61%. There is, however, a tiny contribution of the  $n = 2$  and even higher number states. This is unavoidable in down-conversion based single photon sources; there is a finite probability that neighbouring photon pairs are produced so close to each other that they overlap, thus giving a higher average photon number than 1 within the mode function. For very low gain these higher photon number components become insignificant, but at the same time, of course, the generation rate goes towards zero. With the current gain we have achieved a good compromise between generation rate and low 2-photon contribution to the state. The average trigger detection rate in this measurement series was  $12,800s^{-1}$ . Corrected for the trigger photon losses – the APD detection efficiency of 44%, the total trigger beam path transmission of 14%, and the OPO escape efficiency of 97% – the estimated photon production rate was  $R_{observed} \approx 215,000s^{-1}$ . This figure is close to the theoretically expected production rate in each cavity mode, which, from

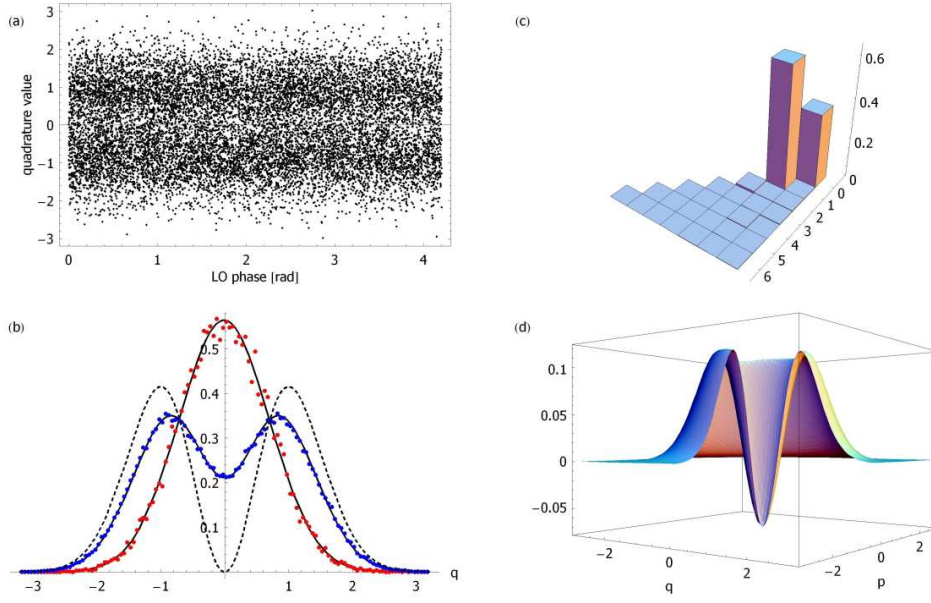


Fig. 3. (Color online) **a**) Part of the recorded quadrature data set with corresponding phases. **b**) Histogram of the distribution of all 180,000 conditional quadrature points (blue) and 40,000 vacuum points (red). The superimposed curves are the theoretical vacuum state distribution, and the single photon distribution fitted to the data with the total efficiency  $\eta$  as the only parameter. The fitted value is  $\eta = 0.625 \pm 0.002$ . The dashed curve is the ideal ( $\eta = 1$ ) single photon distribution. **c**) The density matrix of the state, reconstructed via a maximum likelihood method, and in **d**) the corresponding Wigner function.

eq. (1), is  $R_{theory} = \langle \hat{a}_{\pm}^{\dagger}(t) \hat{a}_{\pm}(t) \rangle = \gamma_{1/2} \epsilon^2 / (1 - \epsilon^2) \approx 200,000 s^{-1}$ . Both of these numbers are, however, too uncertain to be the basis for an estimate of the number of false clicks. The given photon production rate corresponds to a spectral brightness of 1500 photons/s per MHz within the 8 MHz FWHM bandwidth.

The inferred total detection efficiency,  $\eta = 62\%$ , does not fit too well with the calculated value based on independent estimates of the various loss/efficiency contributions, which was as follows. The already mentioned escape efficiency of the OPO was 97%, the transmission towards the homodyne detector was 92%, and the visibility with the LO was 97% leading to an overlap efficiency of  $(97\%)^2$ . On top of these purely optical loss contributions come a specified diode quantum efficiency of 98% and a contribution from the electronic noise of 91% (in the frequency range concerned, the electronic noise level is 10.5 dB below vacuum noise). In total, the estimated efficiency of generation and measurement is  $\eta = 75\%$  – but this number is far from what we observe. A likely explanation for part of this discrepancy might be an insufficient suppression of the uncorrelated frequency modes in the series of trigger filters. As already mentioned, this would lead to a statistical admixture of the thermal state rather than vacuum. There is already a small amount of thermal state admixed due to the dark counts of the APD ( $\sim 100 s^{-1}$ ), but since the thermal state for the low gain is almost indistinguishable from the vacuum, the effect of the thermal state admixture is basically identical to losses (vacuum admixture). Hence, it is also difficult to assert whether the discrepancy between expected and observed efficiency is due to insufficient filtering or unknown sources of loss. Such an addi-

tional source of loss could possibly be the effect of low-frequency classical laser noise which is not completely balanced out in the homodyne setup, since the state selection done by the mode function integration includes all frequencies within the OPO bandwidth. A beginning diode saturation due to too high intensity on the tiny diodes might be another cause. Finally, the temporal mode function, chosen as (3), is not ideally matched to the single photon field and hence some vacuum is admixed to the state on this account. Any fluctuations in the arrival time of the photons would have the same effect.

The Wigner function in Fig. 3(d) clearly has the shape of the single photon Fock state, although mixed with some vacuum. The negative dip has a value of  $W(0,0) = -0.070$  – a clear signature of a non-classical state measured with high efficiency. If we correct the state for the purely measurement related losses (detector quantum efficiency and noise), we get a 70% pure state with a Wigner function dip of  $W(0,0) = -0.12$ . This state is what we obtain after mixing on the beam splitter with the local oscillator, and as such is the state which would be relevant for the storage in an atomic memory, where the quantum state to be stored must be mixed with a strong interaction field [3].

#### 4. Correlation function measurement

Now we demonstrate how the cross correlation function between the two modes of the down-converted field can be extracted from the recorded data. Usually correlation functions are measured via coincidence clicks on photon counting detectors. In [35] each photon counter is replaced with a homodyne detection setup and the  $g^{(2)}(\tau)$  correlation function is calculated from the continuous frequency sideband measurements of the field quadratures. The scheme presented here, which in the essence is similar to the work by Foster et al. [36], is a combination of these two approaches, where one mode is detected by a photon counter and the other by a homodyne setup. We use exactly the same setup and the same data as for the single photon generation and measurement. Figure 4 shows the point-wise variance of the 180,000  $2\mu\text{s}$  long quadrature noise traces, together with a similar variance for the vacuum state. Before taking the variance, the traces have been low-pass filtered by a Lorentz-shaped filter with a 30 MHz cut-off. The increased variance of the conditioned state around the trigger time is evident and consistent with the expected quadrature variance of a single photon state which – in the ideal case – is  $3/2$  in the normalization where the vacuum variance is  $1/2$ . The reason for the lower peak value is partly the limited detection efficiency, but also the effect of including frequency components far outside the OPO bandwidth where there is nothing but vacuum (a frequency filter much narrower than the 30 MHz would decrease the contribution from this vacuum and hence increase the variance, but it would also widen the temporal shape). This signal mode variance conditioned on a trigger photon detection at time  $t_c$  is

$$\langle \Delta \hat{q}_s(\tau)^2 \rangle|_{cond} = \frac{\langle \hat{a}_t^\dagger(t_c) (\hat{q}_s(t_c + \tau))^2 \hat{a}_t(t_c) \rangle}{\langle \hat{a}_t^\dagger \hat{a}_t \rangle} = \frac{1}{2} + \frac{\langle \hat{a}_t^\dagger(t_c) \hat{a}_s^\dagger(t_c + \tau) \hat{a}_s(t_c + \tau) \hat{a}_t(t_c) \rangle}{\langle \hat{a}_t^\dagger \hat{a}_t \rangle}, \quad (4)$$

where we used that the input states are Gaussian with zero mean, and that many correlation terms of the non-degenerate OPO are vanishing, cf. (1). The quadrature operator  $\hat{q}$  is defined as  $\hat{q} \equiv (\hat{a}e^{-i\theta} + \hat{a}^\dagger e^{i\theta})/\sqrt{2}$ , where the phase is made implicit due to the phase-invariance of the state. In order to calculate explicitly the expected variance, the signal and trigger modes,  $\hat{a}_s$  and  $\hat{a}_t$ , must include the detection efficiencies and any transformations – optical or electronic – applied to them, as done by the mode function in (2). For example, the filtering of the trigger field by the filter cavities must be taken into account. For uncorrelated modes (for instance far away from  $t_c$ ), the variance reduces to the thermal state variance  $\langle \Delta \hat{q}_s(\tau)^2 \rangle|_{uncond} = \langle \Delta \hat{q}_s(\tau)^2 \rangle|_{thermal} = 1/2 + \langle \hat{a}_s^\dagger \hat{a}_s \rangle$ . The  $g_{ts}^{(2)}(\tau)$  cross-correlation function is



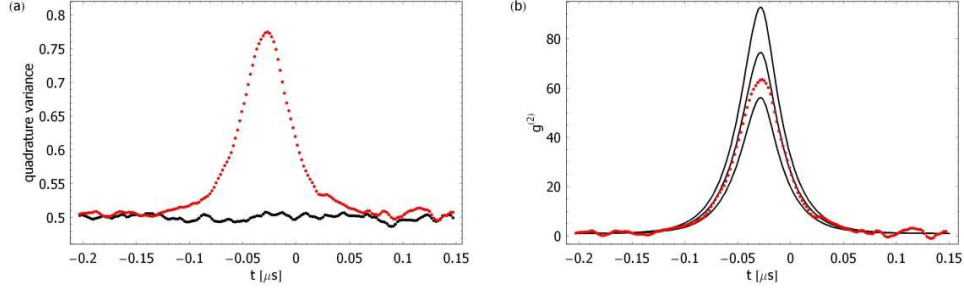


Fig. 4. (Color online) **a)** Variance of the recorded quadrature noise traces for the signal conditioned on a trigger event at  $t = 0$  (red) and for vacuum (black). The traces have been low-pass filtered with a bandwidth of 30 MHz to suppress most of the detector output which lies outside of the field bandwidth. **b)** The cross correlation function,  $g_{ts}^{(2)}(t - t_c)$  (with the trigger time  $t_c = -29$  ns), calculated from the variances in a). Far away from the trigger time the value is 1, but the large values around  $t_c$  demonstrate a strong correlation between the trigger and signal fields. The black curves are the theoretically expected functions for single photon state contents (versus thermal state) of 1, 0.8, and 0.6 (the lowest).

now easily seen to be a simple expression of the quadrature variances

$$g_{ts}^{(2)}(\tau) \equiv \frac{\langle \hat{a}_t^\dagger(t_c) \hat{a}_s^\dagger(t_c + \tau) \hat{a}_s(t_c + \tau) \hat{a}_t(t_c) \rangle}{\langle \hat{a}_t^\dagger \hat{a}_t \rangle \langle \hat{a}_s^\dagger \hat{a}_s \rangle} = \frac{\langle \Delta \hat{q}_s(\tau)^2 \rangle|_{cond} - 1/2}{\langle \Delta \hat{q}_s(\tau)^2 \rangle|_{uncond} - 1/2}. \quad (5)$$

In Fig. 4(b), this  $g_{ts}^{(2)}$  function has been calculated from the variances in Fig. 4(a), where the thermal state variances have been calculated as the mean values of the traces far away from the trigger time. The expression (5) does no longer depend on the signal efficiency, which means that high frequency vacuum contributions play no role in the shape and size of the correlation function. In the figure are also plotted three expected  $g_{ts}^{(2)}$  functions, calculated from a pump parameter  $\varepsilon = 0.09$  and a statistical single photon content of 1, 0.8, and 0.6, respectively, where the remaining parts are made up of the thermal state. The optical filtering of the trigger mode (24 MHz, according to the bandwidth of the narrowest filter cavity) and the digital 30 MHz signal mode filtering have been included in these plots. In principle, since the correlation functions are independent on the signal detection efficiency but depend on the amount of thermal state admixture, it should be possible to find this amount by fitting these theoretical curves to the measurements. However, the uncertainty in the value of the thermal state variance (which is very close to  $1/2$ ) turns into a huge uncertainty in the derived  $g_{ts}^{(2)}$  function – the error bars are so large that they are not displayed in the figure – so that this estimation is meaningless. More precise values would have been attainable if we had made a large number of measurements of the unconditioned thermal state.

## 5. Conclusion

In conclusion, we have presented a high-purity and high-spectral brightness source of heralded single photons, whose narrow bandwidth and clean spatial mode make it very suitable for interactions with an atomic memory. The generated single photons were characterized by homodyne tomography, showing a clearly negative Wigner function. Finally, we demonstrated how the correlation function between two fields can be measured by a combination of instantaneous photon counting and continuous homodyne measurement. The 70% purity of the state

demonstrated here should not be the limit. With some effort a purity of 90% is within reach for the present setup.

This research has been funded in part by EU grants QAP and COVAQIAL. We acknowledge enlightening discussions with Anne E. B. Nielsen and Klaus Mølmer, and the kind assistance of Akira Furusawa in supplying us with the PPKTP crystal.